

Urban Outdoor Propagation Measurements and Channel Models at 6.75 GHz FR1(C) and 16.95 GHz FR3 Upper Mid-Band Spectrum for 5G and 6G

Dipankar Shakya^{†1}, Mingjun Ying^{†2}, Theodore S. Rappaport^{†3}, Peijie Ma[†], Idris Al-Wazani[†], Yanze Wu[†], Yanbo Wang[†], Doru Calin^{*}, Hitesh Poddar[‡], Ahmad Bazzi^{§†}, Marwa Chafii^{§†}, Yunchou Xing[¶], Amitava Ghosh[¶]

[†]NYU WIRELESS, Tandon School of Engineering, New York University, USA

^{*}MediaTek USA Inc., Warren, NJ, USA

[‡]Sharp Laboratories of America (SLA), Vancouver, Washington, USA

[§]Engineering Division, New York University Abu Dhabi, UAE

[¶]NOKIA Standards, Naperville, IL, USA

{¹dshakya, ²yingmingjun, ³tsr}@nyu.edu

Abstract—Global allocations in the upper mid-band spectrum (4–24 GHz) necessitate a comprehensive exploration of the propagation behavior to meet the promise of coverage and capacity. This paper presents an extensive Urban Microcell (UMi) outdoor propagation measurement campaign at 6.75 GHz and 16.95 GHz conducted in Downtown Brooklyn, USA, using a 1 GHz bandwidth sliding correlation channel sounder over 40–880 m propagation distance, encompassing 6 Line of Sight (LOS) and 14 Non-Line of Sight (NLOS) locations. Analysis of the path loss (PL) reveals lower directional and omnidirectional PL exponents compared to mmWave and sub-THz frequencies in the UMi environment, using the close-in PL model with a 1 m reference distance. Additionally, a decreasing trend in root mean square (RMS) delay spread (DS) and angular spread (AS) with increasing frequency was observed. The NLOS RMS DS and RMS AS means are obtained consistently lower compared to 3GPP model predictions. Point data for all measured statistics at each TX-RX location are provided to supplement the models and results. The spatio-temporal statistics evaluated here offer valuable insights for the design of next-generation wireless systems and networks.

Index Terms—FR3, FR1(C), 6G, UMi, outdoor, upper mid-band, delay spread, angular spread, path loss, propagation, channel model

I. INTRODUCTION

The upper mid-band spectrum is as a major candidate for the deployment of cellular wireless services for 5G and 6G communications, with the FR1(C) (4–8 GHz) and Frequency Range 3 (FR3, 7–24 GHz) bands showing promise for increased capacity and coverage [1]–[3]. Recognizing the potential of the upper mid-band frequencies, telecommunications authorities across the world have made allocations in the upper mid-band spectrum for cellular services [1]. Particularly for outdoor urban environments, understanding the physical channel is crucial to drive coexistence with incumbents and facilitate effective air-interface design. The evaluation of path loss, delay and angular spreads are critical for determining the numerology for parameterizing the cellular network design, encompassing

aspects such as sub-carrier spacing, cyclic prefix length for waveform design, or beamforming and beam management [3], [4]. However, there are limited studies analyzing the radio propagation characteristics in the upper mid-band spectrum.

Zhang *et al.* in [3] presented observations for coverage, network design, and showed lower measured RMS delay spread (DS) than predicted by 3GPP models at 6.5 GHz and 15 GHz in an outdoor campus. The observations were based on measurements conducted in [5] using PN sequence transmitted between a signal generator and spectrum analyzer pair with rooftop TX at 12.5 m height and human height RX. 200 MHz BW was used at 6.5 GHz and 1 GHz BW at 15 GHz. Using a 1 m free space reference distance in the close-in (CI) PL model, the PLE in LOS was obtained as 2.07 and 2.01 at 6.5 GHz and 15 GHz, respectively, while NLOS PLEs of 2.38 and 2.59 are observed at 6.5 GHz and 15 GHz, respectively [3], [5]. Investigation of the channel characteristics at 10 GHz with 250 MHz BW in a street-canyon in Berlin with a 3.5 m high TX antenna and 1.5 m RX antenna height revealed PLE of 1.6 in LOS and 2.1 in NLOS using the CI model with 1 m reference distance [6]. Additionally, the mean RMS DS is reported as 21.9 ns in LOS and 37.7 ns in NLOS [6]. Wideband urban channel measurements were carried out around the University of Southern California at 3–18 GHz in 500 MHz steps using a 1 GHz BW frequency-hopped multi-band channel sounder [7]. The LOS PLE was reported to vary between 1.5 to 2 using the floating intercept (FI) [8] (w/α between 48.2 and 55.15 dB) and in NLOS, the PLE was observed between 2.2 and 4.3 (w/α between 22 and 63 dB). The LOS RMS DS was observed between 25–50 ns and 30–140 ns in NLOS for the UMi measurements; In LOS environment, the mean RMS DS is observed to decrease from 46 ns to 29 ns from 3 to 18 GHz [7]. Exploration of channel characteristics at 10.1 GHz with a vector network analyzer spanning 500 MHz BW in outdoor campus of the University of Oulu, resulted in PLEs of 2 in LOS and 3 in NLOS using the CI model and a 1 m reference distance

[9]. Mean RMS DS was observed at 21.45 ns in LOS and 41.29 in NLOS. Additionally, mean angular spread (AS) of arrival (ASA) angles was reported 32.6° in LOS and 59.7° NLOS, whereas mean AS of departure (ASD) angles was reported at 14.9° in LOS and 21.1° in NLOS. Elevation spreads for arrival and departure are reported as 7° and 6.8° in LOS and 13° and 8° in NOS, respectively [9].

This paper presents comprehensive models for path loss, RMS DS, and AS, and compares these statistics with existing 3GPP models and existing results at higher mmWave frequencies. The statistics are generated from an intense measurement campaign conducted around the MetroTech Commons in Brooklyn, New York, during Spring 2024, using a 1 GHz bandwidth sliding correlation channel sounder encompassing 7 LOS and 13 NLOS TX-RX location pairs [1]. The channel measurements reported in this paper corroborate the findings in [4] suggests that 3GPP overestimate the DS in NLOS UMi environments at midband frequencies, and suggests that minor modifications may be needed in terms of numerology compared to 5G NR, while the beam management like beam alignment accuracy, optimal beamwidth selection, and dynamic adaptation of the beam management process may need modifications due to higher number of antenna elements at both gNB and UE, accompanied by lower measured AS [3], [9]. The remainder of the paper is organized starting with the channel sounder system details in Section II. A description of the measurement environment and procedures involved for propagation measurements at each location are noted in Section III. Section IV models the large-scale path loss behavior. Secondary statistics including RMS DS and AS are modeled in Section V, followed by the conclusions.

II. WIDEBAND FR1C/FR3 SLIDING CORRELATION CHANNEL SOUNDER

A sliding correlation based channel sounder was employed for capturing the time-domain channel impulse response. The sliding correlation operation is achieved for pseudo-random noise (PN) sequences transmitted between the channel sounder TX and RX, as described in [1], [10], [11]. The main system features are summarized in Table I.

The RF front-end modules are developed by Mini-circuits as a co-located unit to allow ease of switching between frequency bands. A single band is active at a time, while the other front-end module is powered off [1]. Only one RF cable needs to be moved between the RF front-end modules to switch the operating frequency band. The dual-band RF unit is mounted on a mechanically rotatable gimbal that can sweep the azimuth and elevation planes with one-degree spatial resolution.

A. Calibration

The complete channel sounder calibration is accomplished in three phases: system linearity and power calibration, time calibration, and spatial calibration to achieve accurate capture of MPC power, delay, and directions, as detailed in [1], [12].

Recalibration at the end of the day typically shows differences of under 0.2 dB in the received power [1]. An

TABLE I: SYSTEM PARAMETERS FOR THE UPPER MID-BAND CHANNEL SOUNDER AT NYU WIRELESS [1]

Carrier Frequency	6.75 GHz	16.95 GHz
Free Space PL at 1m reference distance	49 dB	57 dB
Baseband signal	11th order PN sequence (2047 chips)	
TX PN Code Chip Rate	500 Mcps	
RX PN Code Chip Rate	499.9375 Mcps	
Slide factor	8000	
RF BW (Null-to-null)	1 GHz	
TX/RX Antenna Gain	15 dBi	20 dBi
TX/RX Ant. HPBW (Az/EI)	30° / 30°	15° / 15°
TX/RX Antenna Height	4 m / 1.5 m	
Max EIRP used	31 dBm	
Max Measurable Path Loss (at 5 dB SNR)	155.6 dB	159.2 dB
TX Polarization	Vertical (V)/Horizontal (H)	
RX Polarization	Vertical/Horizontal	

active patent-pending time-synchronization method [13] is implemented in the outdoor campaign using precision time protocol (PTP) implemented over a Wi-Fi side link to relay a synchronization pulse between Rubidium clocks at the TX and RX. Additionally, a successive drift correction eliminates any remnant drift through repeated observation of a reference MPC delay [1]. Once the TX and RX are moved to their specified location for measurements, the TX RF front-end is mounted on a mast and raised to 4 m height with reference to the TX horn antenna. The RX antenna is raised to 1.5 m height. Horizontal leveling on both front ends is verified with a spirit level and the 0° spatial reference for both systems is set to the geographical North to complete the spatial calibration.

III. MEASUREMENT ENVIRONMENT AND PROCEDURE

The intense measurement campaign was conducted around the NYU Tandon School of Engineering campus in MetroTech, Brooklyn, NY covering approximately 1 km along Myrtle Avenue. TX and RX locations are indicated in Fig. 1 (a) and (b). TX-RX location pairs measured within the ~180 m open-square configuration of the MetroTech Commons are shown in Fig. 1 (a). Additionally, Fig. 1 (b) shows TX-RX location pairs along Myrtle Avenue, beyond MetroTech Commons, with separation distances ranging from 424 to 880 meters, representing a typical street path for a moving vehicle. All measured TX-RX location details at both 6.75 GHz and 16.95 GHz are tabulated in Table V. The outdoor UMi multipath statistics were derived by analyzing the propagation delay, power, and directions for all multipath components (MPCs) at each TX-RX location, following the process outlined in Table II [1].

IV. LARGE SCALE PATH LOSS MODELS

The PL in directional and omnidirectional contexts are evaluated using a close-in (CI) 1 m free space reference distance model, (1). The CI model describes PL with a single parameter,

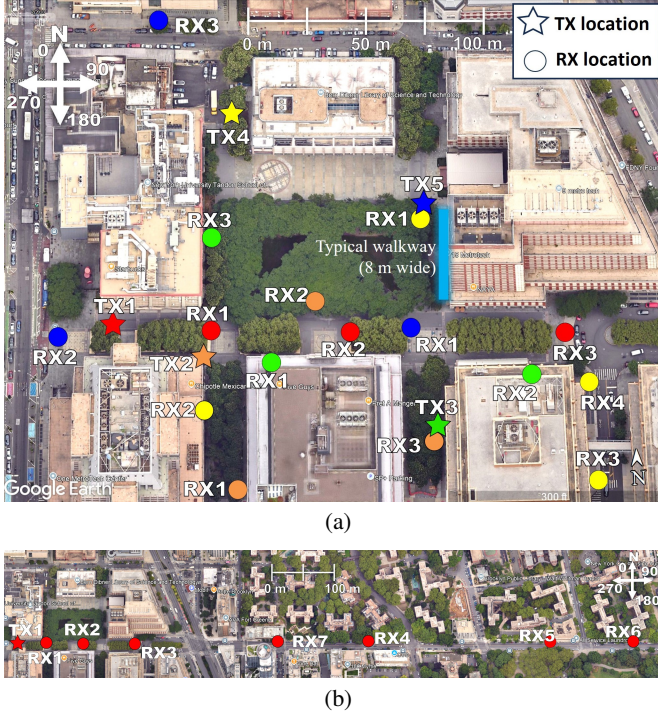


Fig. 1: 6.75 GHz FR1(C) and 16.95 GHz FR3 campaign conducted at the MetroTech Commons in Downtown Brooklyn, NY: (a) Open square of around 200 m. Typical walkways are 8 m wide (one walkway highlighted in sky-blue). (b) Long range measurements for TX1 up to 1 km.

TABLE II: TX/RX ELEVATION ANGLES FOR DIFFERENT RX AZIMUTHAL SWEEPS FOR A FIXED TX AZIMUTH ANGLE AT EACH TX-RX LOCATION [1]

Sweep#	TX elevation	RX elevation
1	TX is kept at <i>boresight</i> elevation	RX is kept at <i>boresight</i> elevation. RX is then swept 360° in the azimuth plane in HPBW steps.
2	TX is kept at <i>boresight</i> elevation	RX is <i>tilted down by one HPBW</i> (30° at 6.75 GHz/ 15° at 16.95 GHz). RX is then swept 360° in the azimuth plane in HPBW steps.
3	TX is kept at <i>boresight</i> elevation	RX is <i>tilted up by one HPBW</i> (30° at 6.75 GHz/ 15° at 16.95 GHz). RX is then swept 360° in the azimuth plane in HPBW steps.
4	TX is <i>tilted down by one HPBW</i> (30° at 6.75 GHz/ 15° at 16.95 GHz).	RX is kept at boresight elevation. RX is then swept 360° in the azimuth plane in HPBW steps.
5	TX is <i>tilted down by one HPBW</i> (30° at 6.75 GHz/ 15° at 16.95 GHz).	RX is <i>tilted down by HPBW</i> (30° at 6.75 GHz/ 15° at 16.95 GHz). RX is then swept 360° in the azimuth plane in HPBW steps.

the path loss exponent (PLE or n), referring to a free-space reference distance, d_0 , as demonstrated in Appendix A of [14].

$$PL^{CI}(f_c, d_{3D}) [\text{dB}] = \text{FSPL}(f_c, 1\text{m}) + 10n \log_{10} \left(\frac{d_{3D}}{d_0} \right) + \chi_\sigma,$$

$$\text{FSPL}(f_c, 1\text{m}) = 32.4 + 20 \log_{10} \left(\frac{f_c}{1 \text{GHz}} \right), \quad (1)$$

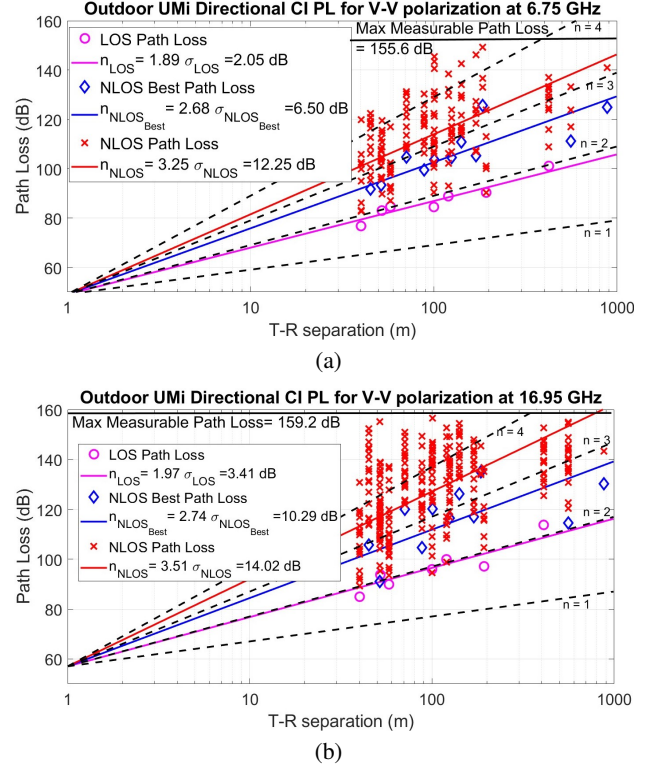


Fig. 2: UMi directional CI PL models and scatter plot for V-V polarization at: (a) 6.75 GHz FR1(C); (b) 16.95 GHz FR3. [T-R separation: 40–880 m]

where $\text{FSPL}(f_c, 1\text{m})$ is obtained for carrier frequency f_c GHz at 1 m, n is the PLE, and χ_σ is large-scale shadow fading (zero-mean Gaussian r.v. with s.d. σ^{CI} in dB) [15].

Fig. 2 presents the directional CI PL models and scatter plots for V-V polarization in an UMi environment at 6.75 GHz and 16.95 GHz. The measurements span T-R separations from 40 to 1000 m. Three scenarios are depicted: LOS, $\text{NLOS}_{\text{Best}}$, and NLOS. The $\text{NLOS}_{\text{Best}}$ PL is calculated when the RX is pointing in the direction with the highest received power. At 6.75 GHz, the PLEs for LOS, $\text{NLOS}_{\text{Best}}$, and NLOS are 1.89, 2.68, and 3.25, respectively. For 16.95 GHz, the PLEs are higher at 1.97, 2.74, and 3.51, respectively. Fig. 3 illustrates the omnidirectional CI PL models and scatter plots for V-V polarization in the same UMi environment and frequency bands. For the 6.75 GHz band, the LOS PLE is 1.79, while the NLOS PLE is 2.56. At 16.95 GHz, the LOS PLE slightly increases to 1.85, and the NLOS PLE is 2.59.

As shown in Table III, the measured PL results are compared with 3GPP models for mid-band, as well as past measurements at higher frequencies (28, 73, and 142 GHz). The measured PLEs at 6.75 and 16.95 GHz are generally lower than those at higher frequencies, particularly for NLOS scenarios, indicating less severe path loss in the FR3 bands than at higher frequencies.

TABLE III: DIRECTIONAL AND OMNIDIRECTIONAL CI PL MODEL PARAMETERS FOR 6.75 AND 16.95 GHz FR1(C) AND FR3 UMI CAMPAIGNS, WITH COMPARISON AT 28, 73 AND 142 GHz CAMPAIGNS

Campaign	Distance (m)	Antenna HPBW (TX/RX)	Directional path loss						Omni path loss			
			LOS		NLOS Best		NLOS		LOS		NLOS	
			n	σ (dB)	n	σ (dB)	n	σ (dB)	n	σ (dB)	n	σ (dB)
6.75 GHz (This work)	40-1000	(30°/30°)	1.89	2.05	2.68	6.5	3.25	12.25	1.79	2.57	2.56	6.53
6.75 GHz (3GPP)	10-135	–	–	–	–	–	–	–	2.1	4	3.19	8.2
16.95 GHz (This work)	40-1000	(15°/15°)	1.97	3.41	2.74	10.29	3.51	14.02	1.85	4.05	2.59	8.78
16.95 GHz (3GPP)	10-339	–	–	–	–	–	–	–	2.1	4	3.19	8.2
28 GHz [11]	31-187	(11°/11°)	2.27	8.15	3.79	7.97	4.13	10.11	2.02	8.98	3.56	8.91
73 GHz [11]	21-170	(7°/15°)	1.92	1.75	2.98	9.36	3.73	11.47	1.87	1.64	2.79	8.56
142 GHz [16]	21-117	(8°/8°)	2.02	2.71	3.07	8.71	3.48	9.53	1.96	2.63	2.92	8.28

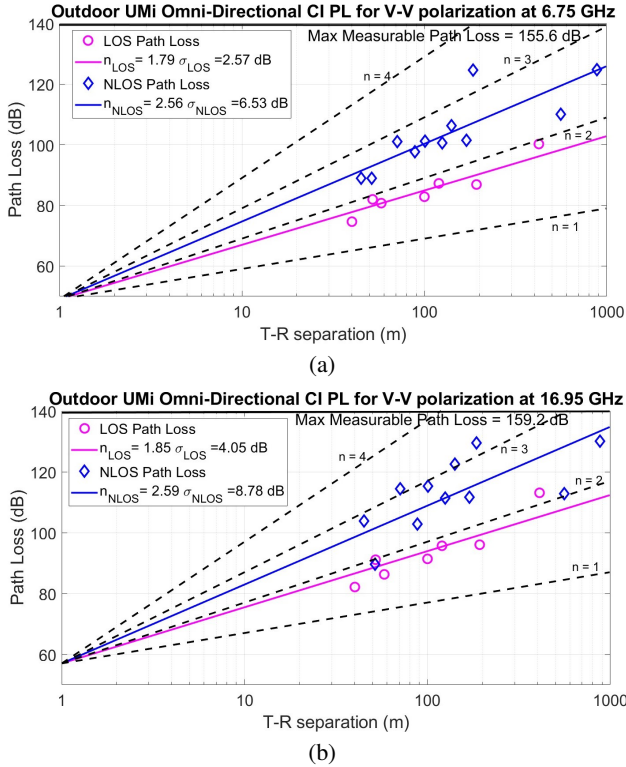


Fig. 3: UMi omnidirectional CI PL models and scatter plot for V-V polarization at: (a) 6.75 GHz FR1(C); (b) 16.95 GHz FR3. [T-R separation: 40–880 m]

V. SPATIO-TEMPORAL STATISTICS

A. Delay Spread Measurement Results

The RMS DS quantifies the temporal dispersion of multipath components in a wideband channel. The RMS DS was evaluated using a power threshold of 25 dB below the PDP maxima or 5 dB above the noise floor. Table IV presents the RMS DS characteristics from 6.75 GHz to 142 GHz for both LOS and NLOS conditions, comparing results with 3GPP models and higher frequency results. For directional measurements at 6.75 GHz, the mean RMS DS is 27 ns in LOS and 35.9 ns in NLOS. At 16.95 GHz, these values are 28.1 ns and 31.7 ns, respectively. The omnidirectional RMS DS, synthesized from directional PDPs [17], shows higher values: 63.5 ns (LOS) and

TABLE IV: RMS DELAY SPREAD CHARACTERISTICS FROM 6.75 GHz TO 142 GHz FOR LOS AND NLOS CONDITIONS.

Frequency (GHz)	6.75	6.75 (3GPP)	16.95	16.95 (3GPP)	28 [16]	73 [11]	142 [11]
Dir RMS DS							
LOS [μ (ns)]	29.1	–	28.1	–	19.3	14.7	3.6
NLOS [μ (ns)]	35.6	–	31.7	–	25.7	23.4	9.2
Omni RMS DS							
LOS [μ (ns)]	62.8	52.7	46.5	42.9	26.7	16.4	15.4
NLOS [μ (ns)]	75.6	111.1	65.8	96.65	46.3	50.8	27.3

74.1 ns (NLOS) at 6.75 GHz, and 46.5 ns (LOS) and 65.8 ns (NLOS) at 16.95 GHz.

Comparing across frequencies, a clear decreasing trend in RMS DS is observed as frequency increases, evident in both directional and omnidirectional measurements for LOS and NLOS scenarios. This trend suggests reduced multipath dispersion at higher frequencies, consistent with findings at mmWave frequencies [11], [16]. The mean values for direct comparison with 3GPP are evaluated in log-scale assuming underlying log-normal distribution. Our measurements at 6.75 GHz and 16.95 GHz generally show slightly higher RMS DS values compared to the 3GPP models in LOS scenarios, while the measured NLOS RMS DS is lower compared to 3GPP model results.

B. Angular Spread Measurement Results

Table VI presents the omnidirectional RMS AS statistics, including azimuth spread of arrival (ASA) and azimuth spread of departure (ASD), evaluated from the measurements. The detailed methodology for deriving these AS parameters is documented in [19]. Following 3GPP model conventions, the AS is characterized using log-normal distributions parameterized by μ and σ , enabling direct comparison with 3GPP model predictions. To ensure statistical comparability with typical UMi scenarios, measurements outside the open square, along the urban street canyon in Fig. 1 (b), beyond 180 m were excluded from the AS analysis as these distant locations exhibited significantly reduced AS.

At 6.75 GHz, the measured omnidirectional RMS ASA shows expected values of 21.5° in LOS and 33.67° in NLOS conditions, which are noticeably lower than the 3GPP model

TABLE V: LARGE SCALE SPATIO-TEMPORAL STATISTICS [18]

Freq.	TX	RX	Loc.	TR Sep.	Omni Abs. PL (V-V)	Omni Abs. PL (V-H)	Mean Dir. DS	Omni DS	Mean Lobe ASA	Omni ASA	Mean Lobe ASD	Omni ASD	Mean Lobe ZSA	Omni ZSA	Mean Lobe ZSD	Omni ZSD	
[GHz]				[m]	[dB]	[dB]	[ns]	[ns]	[°]	[°]	[°]	[°]	[°]	[°]	[°]	[°]	
6.75	TX1	RX1	LOS	40	74.63	84.77	41.1	29.3	23.5	23.5	19.3	24.6	9.0	12.2	2.8	8.6	
		RX2	LOS	100	82.85	106.7	46.5	60.5	14.5	14.5	13.9	22.3	18.2	18.2	1.7	8.5	
		RX3	LOS	193	86.89	104.6	23.5	121.3	6.4	6.4	6.3	65.1	6.4	19.8	2.7	12.9	
		RX4	NLOS	560	110	136.6	2.2	66.4	10.7	10.7	12.9	22.0	4.4	15.4	2.3	9.5	
		RX5	NLOS	880	124.8	-	0.0*	0.0*	5.8	5.8	5.8	5.8	5.8	13.1	5.8	5.8	
		RX6	NLOS	1000													
		RX7	LOS	424	79.2	121.8	37.5	184.6	10.4	10.4	10.5	81.6	4.1	15.4	7.4	13.3	
	TX2	RX1	LOS	58	80.74	95.28	25.2	60.9	18.8	63.0	21.9	24.0	21.5	20.8	3.3	9.8	
		RX2	NLOS	51.5	88.93	107.3	34.6	117.7	13.6	68.7	18.9	35.5	17.4	16.5	3.3	9.8	
		RX3	NLOS	100.9	100.4	125.5	71.4	105.5	18.4	18.4	18.1	65.9	2.6	14.3	5.6	13.9	
	TX3	RX1	NLOS	71	101	117.7	60.4	171.4	34.0	34.0	34.4	36.4	11.7	11.7	7.8	7.8	
		RX2	NLOS	45	88.92	109.2	47.5	55.7	23.8	23.8	39.8	47.8	9.7	12.9	8.8	8.6	
		RX3	NLOS	125	100.6	125.3	24.6	66.5	18.3	55.7	33.4	37.1	9.9	15.9	10.0	9.8	
	TX4	RX1	NLOS	88.7	97.7	117.1	35.4	49.5	16.1	16.1	69.2	70.2	2.3	13.8	7.8	8.1	
		RX2	LOS	120	87.25	110.2	70.3	22.8	10.5	10.5	10.6	13.4	4.3	14.8	4.4	11.4	
		RX3	NLOS	216													
		RX4	NLOS	185	124.5	-	31.0	34.0	12.6	12.6	16.5	16.5	4.5	4.5	3.2	3.2	
	TX5	RX1	LOS	52	81.98	102.8	35.1	26.8	10.8	10.8	11.2	19.1	4.3	15.5	4.4	10.5	
		RX2	NLOS	170	101.5	125.1	31.5	46.2	24.2	24.2	10.5	32.6	3.8	12.6	4.2	12.1	
		RX3	NLOS	141	106.3	129.9	40.0	89.4	46.5	46.5	22.0	75.8	2.3	10.1	7.1	10.7	
	16.95	TX1	RX1	LOS	40	82.14	113.4	35.9	34.0	11.8	11.8	10.9	15.2	5.2	7.3	0.9	4.0
			RX2	LOS	100	91.39	121.4	28.7	56.2	7.2	7.2	8.2	18.7	9.6	9.6	2.4	5.6
			RX3	LOS	193	96.04	124.1	26.5	118.5	6.6	67.0	7.3	57.1	7.6	12.4	1.8	5.6
			RX4	NLOS	560	112.8	138.9	14.7	168.6	10.1	10.1	6.9	78.0	2.7	8.0	4.2	7.7
RX5			NLOS	880	130.1	-	0.0*	0.0*	5.8	5.8	5.8	5.8	5.4	5.4	5.4	5.4	
RX6			NLOS	1000													
RX7			LOS	410	113.1	138.4	65.9	97.9	5.8	5.8	10.4	47.8	5.4	11.5	7.3	9.0	
TX2		RX1	LOS	58	86.3	106.8	46.2	16.9	16.6	16.6	6.7	22.0	3.2	8.3	4.1	8.9	
		RX2	NLOS	51.5	89.61	118.8	94.5	37.3	8.0	8.0	7.5	25.1	7.0	9.6	4.0	7.3	
		RX3	NLOS	100.9	115.2	138.1	104.9	146.2	19.5	19.5	9.3	20.4	6.3	7.6	6.1	9.7	
TX3		RX1	NLOS	71	114.4	141.1	83.7	180.8	20.9	28.0	10.4	28.4	2.9	8.1	4.7	8.4	
		RX2	NLOS	45	103.9	128.6	9.7	34.3	5.6	19.8	10.5	31.4	8.8	12.1	7.1	9.8	
		RX3	NLOS	125	88.8	123.8	25.6	64.5	14.4	33.5	15.0	23.5	11.4	13.6	11.9	11.5	
TX4		RX1	NLOS	88.7	102.9	126.2	19.2	31.9	7.7	33.9	7.3	80.4	4.1	9.9	6.3	8.1	
		RX2	LOS	120	95.46	123.8	34.7	22.1	4.8	46.8	6.3	10.9	8.0	9.8	3.6	7.6	
		RX3	NLOS	216													
		RX4	NLOS	185	129.5	-	18.0	18.0	11.9	11.9	9.9	24.2	4.8	4.8	5.6	5.2	
TX5		RX1	LOS	52	91.11	115.9	86.4	23.6	5.8	5.8	5.8	12.0	5.4	11.6	5.4	8.9	
		RX2	NLOS	170	111.7	-	17.5	28.1	25.6	25.6	9.1	18.5	9.3	9.3	4.2	7.2	
		RX3	NLOS	141	122.5	-	28.9	60.5	28.3	28.3	9.5	47.7	5.5	7.3	3.5	4.2	

*only have one MPC from a single direction at this location.

TABLE VI: ANGULAR SPREAD CHARACTERISTICS MEASURED BY NYU WIRELESS AT 6.75 GHz AND 16.95 GHz IN LOS AND NLOS (T-R SEP. < 180 M) FOR THE UMI ENVIRONMENT AND COMPARISON TO 3GPP MODELS [20].

Metric	Condition	6.75 GHz				16.95 GHz			
		NYU	3GPP	$\mathbb{E}(\text{NYU})$	$\mathbb{E}(\text{3GPP})$	NYU	3GPP	$\mathbb{E}(\text{NYU})$	$\mathbb{E}(\text{3GPP})$
Omni RMS \lg_{ASA} = $\log_{10}(\text{ASA}/1^\circ)$	$\mu_{\lg_{\text{ASA}}}^{\text{LOS}}$	1.28	1.66	21.50°	50.36°	1.20	1.63	17.73°	47.31°
	$\sigma_{\lg_{\text{ASA}}}^{\text{LOS}}$	0.32	0.29			0.32	0.30		
	$\mu_{\lg_{\text{ASA}}}^{\text{NLOS}}$	1.50	1.74	33.67°	62.78°	1.36	1.71	24.13°	59.54°
	$\sigma_{\lg_{\text{ASA}}}^{\text{NLOS}}$	0.23	0.34			0.22	0.36		
Omni RMS \lg_{ASD} = $\log_{10}(\text{ASD}/1^\circ)$	$\mu_{\lg_{\text{ASD}}}^{\text{LOS}}$	1.50	1.16	32.44°	17.54°	1.20	1.15	16.10°	17.14°
	$\sigma_{\lg_{\text{ASD}}}^{\text{LOS}}$	0.15	0.41			0.12	0.41		
	$\mu_{\lg_{\text{ASD}}}^{\text{NLOS}}$	1.60	1.32	41.88°	25.85°	1.49	1.24	32.37°	22.41°
	$\sigma_{\lg_{\text{ASD}}}^{\text{NLOS}}$	0.21	0.43			0.20	0.47		

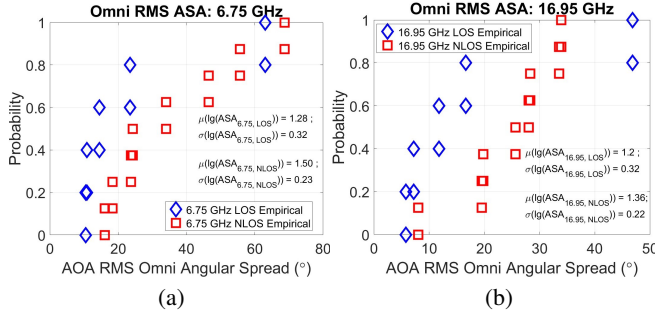


Fig. 4: UMi omnidirectional ASA: (a) 6.75 GHz; (b) 16.95 GHz. [T-R separation: 40–180 m]

predictions of 50.36° and 62.78° , respectively. The 16.95 GHz measurements also yield smaller spreads, with expected values of 17.73° in LOS and 24.13° in NLOS, compared to 3GPP model values of 47.31° and 59.54° . For the omnidirectional RMS ASD, our measurements at 6.75 GHz reveal larger spreads than the 3GPP model, with expected values of 32.44° in LOS and 41.88° in NLOS, compared to 3GPP values of 17.54° and 25.85° , respectively. Similar trends are observed at 16.95 GHz, where measured expected values are 16.10° in LOS and 32.37° in NLOS, versus 3GPP predictions of 17.14° and 22.41° . The measurements consistently show frequency-dependent behavior in AS, with higher frequencies generally exhibiting smaller AS. The observations suggest that current 3GPP models may need revision to closely model the observed AS characteristics. Location-specific spatio-temporal statistics given in point data form, described in [18], are summarized in Table V and follows the detailed approach presented for indoor hotspot in [18].

VI. CONCLUSION

Extensive outdoor propagation measurements at 6.75 GHz and 16.95 GHz conducted in Downtown Brooklyn, USA were presented encompassing 7 LOS and 13 NLOS locations with two outages. The measurements reveal lower PLEs in these bands compared to mmWave frequencies, suggesting better coverage potential for urban deployments. Additionally, a decreasing trend in RMS DS was observed with increasing frequency. RMS AS also showed a decreasing trend at higher frequencies. Compared to 3GPP models, the RMS ASA and NLOS RMS DS were found to be consistently lower at both 6.75 GHz and 16.95 GHz. The results can provide valuable insights for facilitating air-interface and network design for 5G and 6G communications, e.g., for beam management, where beam alignment is a key factor especially for higher number of elements at gNB and different AS values reported.

ACKNOWLEDGMENT

Authors thank Prof. Sundeep Rangan and Prof. Marco Mezzavilla for support with licensing.

REFERENCES

- [1] D.Shakya *et al.*, “Comprehensive FR3 and FR1C upper-mid band propagation measurements and models in Indoor Office environment for 5G and 6G communications,” (*Invited*) *IEEE Open Journal of Comm. Soc.*, pp. 1–13, 2024.
- [2] S. Kang *et al.*, “Cellular wireless networks in the upper mid-band,” *IEEE Open Journal of the Communications Society*, pp. 1–18, 2024.
- [3] J. Zhang *et al.*, “New Mid-Band for 6G: Several Considerations from the Channel Propagation Characteristics Perspective,” *IEEE Communications Magazine*, pp. 1–6, 2024.
- [4] A. A. Zaidi *et al.*, “Waveform and numerology to support 5G services and requirements,” *IEEE Comm. Mag.*, vol. 54, no. 11, pp. 90–98, 2016.
- [5] H. Miao *et al.*, “Sub-6 GHz to mmWave for 5G-Advanced and Beyond: Channel Measurements, Characteristics and Impact on System Performance,” *IEEE Journal on Selected Areas in Communications*, vol. 41, no. 6, pp. 1945–1960, 2023.
- [6] M. Peter *et al.*, “Channel measurement and modeling for 5G urban microcellular scenarios,” *Sensors*, vol. 16, no. 8, p. 1330, 2016.
- [7] V. Kristem *et al.*, “Outdoor wideband channel measurements and modeling in the 3–18 GHz band,” *IEEE Transactions on Wireless Communications*, vol. 17, no. 7, pp. 4620–4633, 2018.
- [8] S. Sun *et al.*, “Propagation path loss models for 5G urban micro and macro-cellular scenarios,” in *2016 IEEE 83rd Vehicular Technology Conference (VTC Spring)*. IEEE, 2016, pp. 1–6.
- [9] A. Roivainen *et al.*, “Parametrization and validation of geometry-based stochastic channel model for urban small cells at 10 GHz,” *IEEE Trans. Ant. and Prop.*, vol. 65, no. 7, pp. 3809–3814, 2017.
- [10] D. Shakya *et al.*, “A Wideband Sliding Correlation Channel Sounder in 65 nm CMOS: Evaluation Board Performance,” *IEEE Transactions on Circuits and Systems II: Express Briefs*, vol. 68, no. 9, pp. 3043–3047, 2021.
- [11] D.Shakya *et al.*, “Radio Propagation Measurements and Statistical Channel Models for Outdoor Urban Microcells in Open Squares and Streets at 142, 73, and 28 GHz,” *IEEE Trans. Ant. and Prop.*, pp. 1–15, Feb 2024.
- [12] —, “Propagation measurements and channel models in Indoor Environment at 6.75 GHz FR1(C) and 16.95 GHz FR3 Upper mid-band Spectrum for 5G and 6G,” in (*Accepted*) *IEEE GLOBECOM 2024*, 2024, pp. 1–6.
- [13] D. Shakya, H. Poddar, and T. S. Rappaport, “A sub-terahertz sliding correlator channel sounder with absolute timing using precision time protocol over wi-fi,” in *IEEE GLOBECOM 2023*, 2023, pp. 5793–5798.
- [14] G. R. Maccartney *et al.*, “Indoor office wideband millimeter-wave propagation measurements and channel models at 28 and 73 GHz for ultra-dense 5G wireless networks,” *IEEE access*, pp. 2388–2424, 2015.
- [15] T. S. Rappaport *et al.*, “Wideband millimeter-wave propagation measurements and channel models for future wireless communication system design,” *IEEE Transactions on Communications*, vol. 63, no. 9, pp. 3029–3056, 2015.
- [16] Y. Xing, T. S. Rappaport, and A. Ghosh, “Millimeter wave and sub-thz indoor radio propagation channel measurements, models, and comparisons in an office environment,” *IEEE Communications Letters*, vol. 25, no. 10, pp. 3151–3155, 2021.
- [17] S. Sun *et al.*, “Synthesizing omnidirectional antenna patterns, received power and path loss from directional antennas for 5G millimeter-wave communications,” in *2015 IEEE GLOBECOM*, 2015, pp. 1–7.
- [18] T. S. Rappaport, D. Shakya, and M. Ying, “Point data for site-specific mid-band radio propagation channel statistics in the indoor hotspot (InH) environment for 3GPP and Next Generation Alliance (NGA) channel modeling,” in (*Submitted*) *IEEE International Communications Conference (ICC) 2025*, 2025, pp. 1–6.
- [19] D.Shakya *et al.*, “Angular Spread Statistics for 6.75 GHz FR1(C) and 16.95 GHz FR3 Mid-Band Frequencies in an Indoor Hotspot Environment,” in (*Submitted*) *IEEE WCNC 2024*, 2024, pp. 1–6.
- [20] 3GPP, “Study on channel model for frequencies from 0.5 to 100 GHz (Release 16),” *3GPP TR 38.901 V16.1.0 (2019-12)*, pp. 1–101, Dec 2019.